

Probing Inelastic Dark Matter via Cosmic-Ray Upscattering in NGC 1068

Eung Jin Chun,^{1,*} Sanjoy Mandal,^{1,†} and Abhishek Roy^{2,3,‡}

¹*Korea Institute for Advanced Study, Seoul 02455, Korea*

²*Center for Quantum Spacetime, Sogang University,*

35 Baekbeom-ro, Mapo-gu, Seoul, 121-742, South Korea

³*Department of Physics, Sogang University, 35 Baekbeom-ro, Mapo-gu, Seoul, 121-742, South Korea*

We study constraints on sub-GeV inelastic dark matter (iDM) from cosmic-ray (CR) cooling in the active galactic nucleus (AGN) NGC 1068. In dense dark matter (DM) spikes surrounding supermassive black holes, high-energy CR protons can efficiently lose energy through scatterings with dark matter particles. We consider a minimal vector-portal iDM framework and consistently include both elastic and deep inelastic scattering (DIS) contributions to the CR energy-loss rate. We find that DIS processes dominate at high momentum transfer and substantially enhance the DM-induced cooling effect. By requiring the resulting cooling timescale to remain compatible with the observed Standard Model cooling in NGC 1068, we derive constraints on the iDM parameter space. Our results demonstrate that AGN cosmic-ray cooling probes previously unexplored regions of sub-GeV iDM parameter space inaccessible to current direct-detection experiments.

I. INTRODUCTION

The presence of dark matter (DM) in galaxies and galaxy clusters is well established by diverse astrophysical and cosmological observations, yet its fundamental particle nature remains unknown [1–3]. Weakly interacting massive particles (WIMPs) are compelling dark matter candidates [4, 5] because of their weak-scale interactions, natural thermal production in the early universe, and strong motivation from extensions of the Standard Model. However, the absence of definitive detection has shifted focus toward a wider class of candidates, particularly in the sub-GeV mass range. Yet conventional direct detection experiments rapidly lose sensitivity in this regime due to kinematic threshold limitations [6–14]. Several approaches have been proposed to extend direct detection sensitivity to sub-GeV dark matter, including boosted components produced through gravitational effects or scatterings with protons, electrons, or neutrinos in astrophysical environments [15–29].

There exists a class of sub-GeV dark matter models in which present-day annihilation is suppressed due to non-standard evolution mechanisms, such as number-changing $3 \rightarrow 2$ processes in the dark sector [30–32], asymmetric dark matter [33–35], and freeze-in production [36, 37]. As a result, this class of light dark matter can be probed only through direct detection and accelerator experiments.

A particularly important framework in this context is inelastic dark matter (iDM) [38–40] which was initially introduced to account for the anomalous observations reported by the DAMA collaboration [41]. Since then, iDM has developed into a well-motivated paradigm for sub-GeV thermal dark matter interacting via a vector mediator [42–46]. In this scenario, the dark matter spectrum consists of states with a small mass splitting, leading to distinctive experimental signatures. A defining feature of these models is the presence of off-diagonal interactions between the ground state, χ_1 , and a slightly heavier excited state, χ_2 with $m_{\chi_2} > m_{\chi_1}$. This structure leads to kinematic suppression of dark matter–nucleon scattering rates in present-day direct detection experiments. As a result, iDM models are only weakly constrained by direct detection experiments, particularly when the dark matter mass lies in the sub-GeV range and the mass splitting is relatively large [18, 38, 47–61]. This motivates the exploration of extreme astrophysical environments that may provide enhanced sensitivity to the non-annihilating sub-GeV DM scenarios.

* ejchun@kias.re.kr

† smandal@kias.re.kr

‡ abhishek@sogang.ac.kr

Active galactic nuclei (AGNs) are powerful environments that efficiently accelerate cosmic rays (CRs), where accretion onto a supermassive black hole (SMBH) drives jets, shocks, and turbulent magnetic fields that boost particles to ultra-high energies [62]. In these environments, accelerated CRs—primarily protons—can interact with ambient matter (pp interactions) or radiation fields ($p\gamma$ interactions), producing secondary particles such as pions [63]. The decay of these pions leads to high-energy gamma rays and neutrinos, making AGNs promising multimessenger sources. The CR protons also cool through various other SM processes like synchrotron, inverse Compton, Bethe-Heitler pair production processes and adiabatic losses. For AGNs such as, NGC 1068 [64, 65] and TXS 0506+056 [66–70], detailed multimessenger observations and modeling are available, allowing us to assess the energy dependence of cooling times. Also SMBH at the Galactic Center (GC) can enhance the surrounding DM density, forming a steep spike over the cosmic time as its gravity pulls in and compresses the halo beyond standard predictions [71–73]. As CRs propagate through these dense DM environments, energy transfer from CRs to DM can induce significant cooling effects, making AGNs promising laboratories for probing DM–proton and DM–electron interactions in the sub-GeV regime [74–78].

In this work, we focus primarily on NGC 1068, which provides stronger and more robust sensitivity to iDM compared to blazar systems such as TXS 0506+056. This is mainly due to its dense, proton-dominated environment and the presence of ultra-high-energy CR protons spanning energies from approximately 10^2 to 10^7 GeV. Such a broad CR spectrum enables efficient energy transfer to DM particles and substantially enhances CR cooling through DM upscattering. By contrast, TXS 0506+056 is largely characterised by CR electrons with a comparatively narrower energy range, limiting the maximum transferable energy and suppressing the overall cooling effect. Consequently, proton-induced cooling in NGC 1068 leads to significantly stronger and more reliable constraints on iDM parameter space.

We consider a minimal vector-portal iDM framework in which DM interacts with protons through off-diagonal couplings. Previous studies of sub-GeV DM scattering have primarily focused on elastic processes described by dipole form factors. However, Ref. [76] demonstrated that this treatment becomes inadequate at high proton energies, where the internal structure of the proton can no longer be neglected and deep inelastic scattering (DIS) channels become important. Therefore, analyses restricted to low momentum transfer fail to provide reliable constraints in the high-energy CR regime relevant for AGNs. Motivated by this observation, we consistently include both elastic and DIS contributions to CR–DM scattering when evaluating the CR cooling timescale.

Finally, throughout this work we assume that χ_1 constitutes the present-day DM component, while remaining agnostic about the precise mechanism responsible for generating the observed relic abundance. Viable scenarios include co-annihilation or co-scattering mechanisms involving heavier dark-sector states [79–81], as well as non-standard cosmological histories such as early matter domination or kination-dominated eras [82–88]. Since these possibilities can naturally reproduce the observed DM abundance while leaving the present phenomenology largely unchanged, our analysis is intended to remain broadly applicable to a wide class of iDM realisation.

II. BSM COOLING OF CRS IN AGN

Multimessenger data from NGC 1068 enable us to estimate the energy-dependent cooling times of CR protons, dominated by Standard Model processes such as pp and $p\gamma$ interactions, as well as Bethe–Heitler pair production [89–91]¹. For NGC 1068, detailed multimessenger observations and modeling are available, allowing us to evaluate the energy dependence of the cooling times. The behaviors of the cooling timescales with the CR energy is shown by black solid line in Fig. 2.

Furthermore, it has been suggested that the adiabatic growth of a SMBH can give rise to a DM spike in its surrounding region [71–73]. Starting from an initial power-law profile $\rho(r) = \rho_0 (r/r_0)^{-\gamma}$, the distribution evolves

¹ Specifically, for proton energies $T_p \lesssim 10^4$ GeV, cooling is dominated by pp interactions with the ambient gas. In the intermediate range $T_p \sim 10^4$ – 10^6 GeV, Bethe–Heitler pair production becomes significant, while for $T_p \gtrsim 10^6$ GeV, energy losses are primarily driven by $p\gamma$ interactions [92].

into:

$$\rho_{\text{sp}}(r) = \rho_R g_\gamma(r) \left(\frac{R_{\text{sp}}}{r} \right)^{\gamma_{\text{sp}}}, \quad (1)$$

where $R_{\text{sp}} = \alpha_\gamma r_0 (M_{\text{BH}}/(\rho_0 r_0^3))^{\frac{1}{3-2\gamma}}$ is the size of the spike, and $\gamma_{\text{sp}} = (9 - 2\gamma)/(4 - \gamma)$. Further, $g_\gamma(r) \approx (1 - \frac{4R_S}{r})$, while ρ_R is a normalization factor, chosen to match the density profile outside of the spike, $\rho_R = \rho_0 (R_{\text{sp}}/r_0)^{-\gamma}$. This density profile vanishes at $4R_S$, which represents a conservative approximation. We consider that the initial DM distribution follows an NFW profile [93, 94], with $\gamma = 1$, resulting in a spike with $\gamma_{\text{sp}} = 7/3$ and $\alpha_\gamma = 0.122$. For the scale radius and SMBH mass of NGC 1068, we take $r_0 = 10$ kpc and $10^7 M_\odot$, respectively. Note that if DM undergoes self-annihilation, the density in the innermost region of the spike is limited and saturates at $\rho_{\text{sat}} = \frac{m_{\text{DM}}}{\langle \sigma v \rangle t_{\text{BH}}}$, where $\langle \sigma v \rangle$ is the velocity-averaged annihilation cross section and t_{BH} denotes the age of the central SMBH which we considered to be 10^{10} yr for NGC 1068. We find that the average density of asymmetric or non-annihilating DM particles in the corona of NGC 1068 is $\langle \rho_{\text{DM}} \rangle \sim 5 \times 10^{18}$ GeV/cm³, indicating that the DM density can be extremely high in the region where high-energy CR protons are produced.

As CRs pass through this DM spike, they scatter off DM particles. When the scattering cross section is sufficiently large, this leads to efficient CR cooling, which can in turn modify the high-energy neutrino and gamma-ray fluxes emitted by these sources. As a result, observations of neutrinos and gamma rays offer powerful constraints on CR cooling driven by DM–proton interactions [74]. The BSM cooling timescale due to DM–proton scattering is given by [95]

$$t_{\chi_1 p} = \left[-\frac{1}{E} \left(\frac{dE}{dt} \right)_{\chi_1 p} \right]^{-1}, \quad (2)$$

where E is the CR energy and $\dot{E}_{\chi_1 p} \equiv \left(\frac{dE}{dt} \right)_{\chi_1 p}$ is the energy loss rate due to CR–DM collisions, defined as

$$\dot{E}_{\chi_1 p} = -\frac{\langle \rho_{\chi_1} \rangle}{m_{\chi_1}} \int_{T_{\text{DM}}^{\text{min}}}^{T_{\text{DM}}^{\text{max}}} dT_{\text{DM}} (T_{\text{DM}} + \delta_{\text{DM}}) \frac{d\sigma_{\chi_1 p \rightarrow \chi_2 X}}{dT_{\text{DM}}}, \quad (3)$$

where $\langle \rho_{\chi_1} \rangle$ is the average density of DM particles in the region of CR production. $d\sigma_{\chi_1 p \rightarrow \chi_2 X}/dT_{\text{DM}}$ is the differential DM–proton cross section, $T_{\text{DM}}^{\text{max}}$ ($T_{\text{DM}}^{\text{min}}$) is the maximal (minimal) allowed value for the upscattered DM kinetic energy T_{DM} in a collision with proton with kinetic energy $T_p = E_p - m_p$. The functional form of the differential distributions $d\sigma_{\chi_1 p \rightarrow \chi_2 X}/dT_{\text{DM}}$ differs fundamentally between elastic ($X = p$)² and deep inelastic scattering (DIS; $X = \text{quarks}$) processes. The kinematics energy transfer $T_{\text{DM}}^{\text{min/max}}$ also differs depending on the type of processes.

The functional form of the differential distribution for both elastic scattering and DIS depends on the underlying particle physics model. We consider a simplified dark sector consisting of a vector mediator Z' , a stable fermion DM state χ_1 with mass m_{χ_1} , and a heavier fermion χ_2 with mass $m_{\chi_1} + \delta_{\text{DM}}$. The interaction between the SM and the dark sector is taken to be of the form [38–40]

$$\mathcal{L} = \left[g_\chi \bar{\chi}_1 \gamma^\mu \chi_2 Z'_\mu + \text{h.c.} \right] + \sum_f g_f \bar{f} \gamma^\mu f Z'_\mu, \quad (4)$$

where g_χ and g_f are the coupling constants of the Z' to the dark sector and SM fermions, respectively. We assume that Z' couples equally to protons and neutrons, $g_p = g_n = g_q$, and set other SM couplings to zero. When CR protons transfer only a small momentum to DM, such that $Q^2 \ll 1$ GeV² (where $Q^2 = -q^2 = -(p - p')^2$, with p and p' denoting the four-momenta of the initial- and final-state protons, respectively), the proton can effectively be treated as a point-like particle and the effects of its internal structure remain negligible. As the momentum transfer increases,

² Traditionally, the process $\chi_1 p \rightarrow \chi_2 p$ is classified as inelastic scattering since the final-state masses differ from the initial-state masses. However, in this work we refer to it as elastic scattering to distinguish it from DIS.

however, the nucleon substructure becomes increasingly important, for example through its charge and magnetization distributions. In this region, the proton- Z' interaction can be defined by the electromagnetic form factors $F_1(Q^2)$ and $F_2(Q^2)$ [96],

$$\langle N(p') | \sum_q g_q \bar{q} \gamma^\mu q Z'_\mu | N(p) \rangle = g_p Z'_\mu \bar{N} \Gamma^\mu N, \quad \text{with} \quad \Gamma^\mu = \gamma^\mu F_1(Q^2) + \frac{i}{2m_p} \sigma^{\mu\nu} q_\nu F_2(Q^2), \quad (5)$$

At low Q^2 , the Pauli form factor F_2 is generally suppressed by $\mathcal{O}(q/m_p)$, whereas the Dirac form factor F_1 can be accurately approximated using the dipole form: $F_1(Q^2) = (1 + Q^2/\Lambda^2)^{-2}$ with $Q^2 = 2m_{\chi_1} T_{\text{DM}} - \delta_{\text{DM}}^2$ and $\Lambda = 770$ MeV. At higher momentum transfer, F_2 becomes non-negligible and the dipole form fails. Hence one need to therefore retain both form factors³. As a result, we obtain the differential cross section of DM-proton elastic scattering as,

$$\frac{d\sigma_{\chi p}}{dT_{\text{DM}}} = \frac{|\overline{\mathcal{M}}|^2}{32\pi m_\chi T_p (T_p + 2m_p)} = \frac{g_p^2 g_\chi^2}{8\pi T_p (T_p + 2m_p) (Q^2 + m_{Z'}^2)^2} \times [(F_1(Q^2) + F_2(Q^2))^2 \mathcal{K}_1 + (1 + \tau) F_2(Q^2)^2 \mathcal{K}_2], \quad (6)$$

where $\tau = Q^2/(4m_p^2)$ and the function $\mathcal{K}_{1,2}$ are given as,

$$\mathcal{K}_1 = -2m_{\chi_1}^2 T_{\text{DM}} - T_{\text{DM}}(2m_p^2 + \delta_{\text{DM}}^2) + m_{\chi_1}(4E_p^2 - 4E_p T_{\text{DM}} + 2T_{\text{DM}}^2 - 4E_p \delta_{\text{DM}} + \delta_{\text{DM}}^2), \quad (7)$$

$$\mathcal{K}_2 = m_{\chi_1}(2E_p - \delta_{\text{DM}})(2(E_p - T_{\text{DM}}) - \delta_{\text{DM}}) + \frac{1}{2} T_{\text{DM}}(\delta_{\text{DM}}^2 - 4m_p^2). \quad (8)$$

This expression allows one to evaluate the energy-loss rate via Eq. 2, which in turn determines the CR cooling timescale where the maximum and minimum upscattered DM kinetic energy are given as,

$$T_{\text{DM}}^{\text{min/max}} = \frac{E_p + m_{\chi_1}}{2s} \left[s + (m_{\chi_1} + \delta_{\text{DM}})^2 - m_p^2 \pm \frac{\sqrt{E_p^2 - m_p^2}}{E_p + m_{\chi_1}} \lambda^{\frac{1}{2}} \left(s, m_p^2, (m_{\chi_1} + \delta_{\text{DM}})^2 \right) \right] - (m_{\chi_1} + \delta_{\text{DM}}), \quad (9)$$

where $s = m_p^2 + m_{\chi_1}^2 + 2m_{\chi_1} E_p$.

At sufficiently high proton energies, DM-proton scattering is dominated by DIS. Within the parton model, the nucleon is treated as a collection of quasi-free, spin-1/2, point-like partons, and the DM-proton DIS process is approximated as an incoherent sum of elastic DM-parton scatterings, $\chi_1(k) + q(xP) \rightarrow \chi_2(k') + q(p')$, where x is the momentum fraction carried by the struck parton. In the rest frame of DM, the differential DIS cross section reads,

$$\frac{d\sigma_{\chi p}}{dT_{\text{DM}}} = \sum_q \int_{x_{\text{min}}}^1 dx f_q(x, Q^2) \frac{d\hat{\sigma}}{dT_{\text{DM}}}, \quad (10)$$

where the partonic cross section is

$$\frac{d\hat{\sigma}}{dT_{\text{DM}}} = \frac{m_{\chi_1}}{8\pi \lambda(\hat{s}, m_q^2, m_{\chi_1}^2)} \frac{2g_q^2 g_\chi^2}{(Q^2 + M_{Z'}^2)^2} \left[(Q^2 + \delta_{\text{DM}}^2)(Q^2 - 2m_q^2 - 4xE_p m_{\chi_1}) - 2m_{\chi_1}^2 (Q^2 + 4xE_p(\delta_{\text{DM}} - xE_p)) \right], \quad (11)$$

where $Q^2 = -\hat{t} = -\delta_{\text{DM}}^2 + 2m_{\chi_1} T_{\text{DM}}$ and $\hat{s} = m_q^2 + m_{\chi_1}^2 + 2xm_{\chi_1} E_p$. The parton distribution function $f_q(x, Q^2)$ describes the probability of finding a parton carrying a momentum fraction x of the proton. We only take the partonic contributions from up and down quarks. For this we considered the CT18nnlo set implemented in the LHAPDF package [99]. The lower limit on x is fixed by the threshold condition $\hat{s} > (m_q + m_{\chi_1} + \delta_{\text{DM}})^2$,

$$x_{\text{min}} = \frac{m_q + \delta_{\text{DM}}}{E_p} + \frac{\delta_{\text{DM}}}{2E_p m_{\chi_1}} (\delta_{\text{DM}} + 2m_q). \quad (12)$$

³ It is often convenient to parameterize the form factors F_1 and F_2 in terms of the Sachs form factors G_E^p and G_M^p , which independently characterize the electric and magnetic distributions of the proton [97, 98].

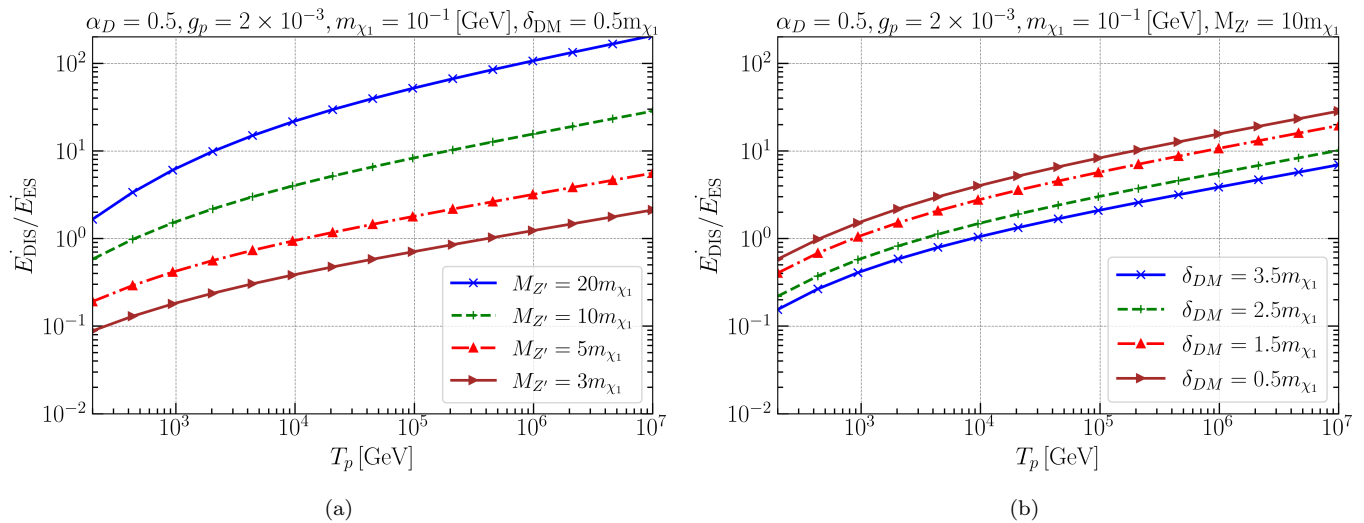


FIG. 1: Ratio of DIS to elastic scattering (ES) energy loss rate $\dot{E}_{\text{DIS}}/\dot{E}_{\text{ES}}$ as a function of proton kinetic energy in CRs for fixed DM mass $m_{\chi_1} = 0.1$ GeV. The left and right panel shows the impact on this ratio due to mediator mass ($M_{Z'}$) and mass splitting (δ_{DM}), respectively.

The maximum and minimum upscattered DM kinetic energy are given as

$$T_{\text{DM}}^{\text{min/max}} = \frac{x E_p + m_{\chi_1}}{2\hat{s}} \left[\hat{s} + (m_{\chi_1} + \delta_{\text{DM}})^2 - m_q^2 \pm \frac{x \sqrt{E_p^2 - m_p^2}}{x E_p + m_{\chi_1}} \lambda^{\frac{1}{2}} \left(\hat{s}, m_q^2, (m_{\chi_1} + \delta_{\text{DM}})^2 \right) \right] - (m_{\chi_1} + \delta_{\text{DM}}). \quad (13)$$

Note that the maximum momentum transfer in both the elastic scattering and DIS cases is given by $Q_{\text{max}}^2 = -\delta_{\text{DM}}^2 + 2m_{\chi_1} T_{\text{DM}}^{\text{max}}$. For elastic scattering, the maximum DM kinetic energy satisfies $T_{\text{DM}}^{\text{max}} < T_p$. In contrast, for DIS processes, the hadronization of the final state relaxes the momentum-transfer constraint, allowing nearly the full proton energy to be transferred to the DM particle, i.e. $T_{\text{DM}}^{\text{max}} \approx T_p$. Consequently, one obtains $Q_{\text{max, DIS}}^2 > Q_{\text{max, ES}}^2$, and this enhancement plays a crucial role in making the DIS contribution significantly larger than the elastic scattering contribution.

In our analysis, we include both the elastic and DIS contributions to the cooling timescale. To derive constraints on the iDM model, we impose the CR cooling condition $t_{\chi_1 p} \leq C t_{\text{SM}}$ to exclude regions of parameter space in which the cooling proceeds too rapidly. The factor C is model dependent parameter and for NGC 1068 it was estimated to vary in the range $0.1 \leq C \leq 1$ [74]. For our calculations, we adopt a conservative value of $C = 0.1$.

III. RESULTS AND DISCUSSION

To compare the contributions of elastic scattering and DIS to the CR cooling rate, we evaluate the energy loss associated with each process focusing on sub-GeV DM with negligible present day annihilation. Fig. 1 shows the ratio of DIS to elastic scattering (ES) energy loss rate $\dot{E}_{\text{DIS}}/\dot{E}_{\text{ES}}$ as function of proton kinetic energy in CRs where we fixed the DM mass as $m_{\chi_1} = 0.1$ GeV. The left panel shows the dependence on the mediator mass $M_{Z'}$ at fixed mass splitting $\delta_{\text{DM}} = 0.5 m_{\chi_1}$, while the right panel shows the dependence on the mass splitting at fixed mediator mass $M_{Z'} = 10 m_{\chi_1}$. It is evident that both $M_{Z'}$ and δ_{DM} play important roles in determining the scattering cross section and, consequently, the CR energy-loss rates. In both panels, the DIS contribution increases monotonically with T_p , independent of $M_{Z'}$ or δ_{DM} , reflecting the fact that larger T_p implies larger momentum transfer Q^2 . We also find that a larger mediator mass $M_{Z'}$ causes DIS to dominate at lower values of T_p . This can be understood from the propagator factor $(Q^2 + M_{Z'}^2)^{-2}$, which controls both the elastic and DIS cross sections. For small $M_{Z'}$, this propagator provides

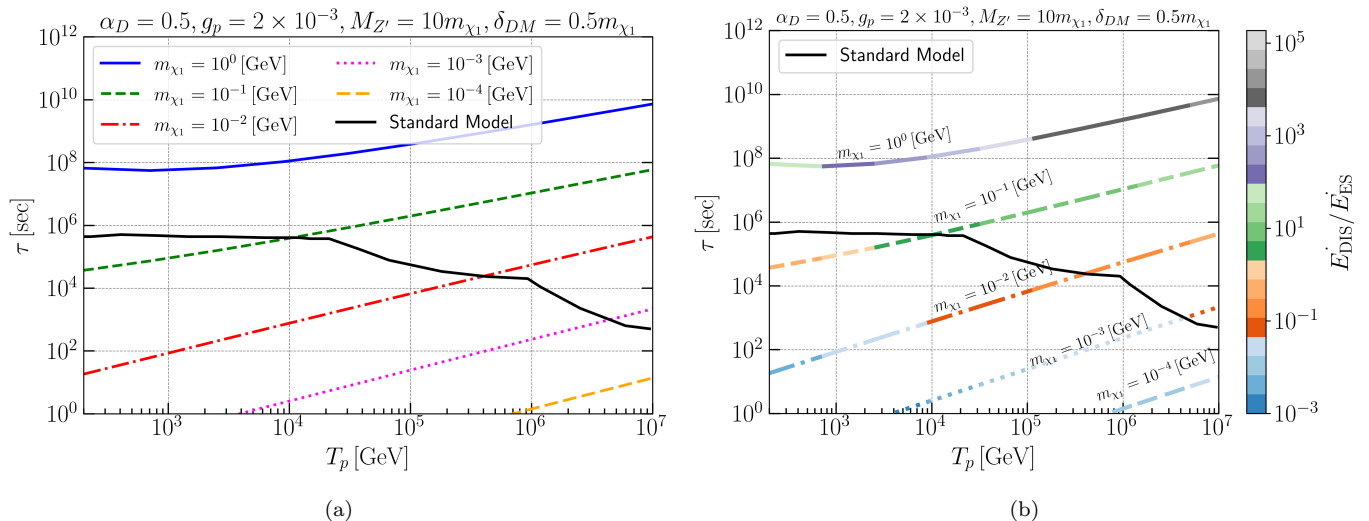


FIG. 2: Cooling timescales from CR protons scattering with DM, in terms of proton energy T_p , compared with those from SM processes for different DM masses. We fix the mass splitting between the two DM states to be $\delta_{\text{DM}} = 0.5 m_{\chi_1}$ and choose the mediator mass as $M_{Z'} = 10 m_{\chi_1}$. The right panel is identical to the left panel, with the color bar indicating the DIS contribution.

a stronger enhancement in the elastic regime ($Q^2 < 1 \text{ GeV}^2$) compared to the DIS regime ($Q^2 > 1 \text{ GeV}^2$). More specifically, once $Q^2 \gtrsim 1 \text{ GeV}^2$ (this will require some minimum value of T_p for fixed m_{χ_1} and δ_{DM}), DIS invariably dominates the energy loss, even for light mediators. This apparent tension with the corresponding cross-section ratios is resolved by the kinematic advantage of DIS: while elastic scattering transfers only a fraction of the proton energy, DIS can lead to nearly complete energy deposition through hadronic fragmentation. The right panel illustrates that, for fixed DM and mediator masses, increasing the mass splitting suppresses the DIS contribution, which can again be understood from the momentum-transfer relation $Q^2 = -\delta_{\text{DM}}^2 + 2 m_{\chi_1} T_{\text{DM}}$.

Fig. 2 shows the dependence of the cooling timescale on the DM mass with the mediator mass and mass splitting fixed to $M_{Z'} = 10 m_{\chi_1}$ and $\delta_{\text{DM}} = 0.5 m_{\chi_1}$. The SM cooling timescale is shown as the solid black line for reference. As m_{χ_1} increases, the DM number density decreases at fixed average density $\langle \rho_{\chi_1} \rangle$, resulting in longer cooling timescales or equivalently smaller interaction rates. Consequently, lighter DM masses yield stronger constraints. In particular, for $m_{\chi_1} \sim 10^{-2} \text{ GeV}$, the DM-induced cooling can dominate over the SM cooling channels for $T_p \lesssim 10^6 \text{ GeV}$. The timescales also increase with T_p since scattering becomes inefficient at large-momenta transfer. For low DM masses, the momentum transfer remains small and the DIS contribution to the energy-loss rate is weak, so elastic scattering dominates. In contrast, increasing m_{χ_1} leads to larger momentum transfer, which enhances the DIS contribution relative to the elastic channel. Consequently, the ratio $\dot{E}_{\text{DIS}}/\dot{E}_{\text{ES}}$ increases systematically with DM mass, as indicated by the color bar in the right panel of Fig. 2.

In light of the above discussion, we see that for certain regions of the iDM parameter space, the cooling timescales can become comparable to, or even shorter than, the SM cooling timescale at the relevant energies, in conflict with observations. We also find that the inclusion of DIS systematically reduces the cooling timescales across the entire kinetic-energy range. The iDM model has five free parameters: the DM mass m_{χ_1} , the mass splitting δ_{DM} , mediator mass $M_{Z'}$, and the mediator coupling to the proton g_p and the dark sector $\alpha_D = g_{\chi}^2/4\pi$, which we fix to $\alpha_D = 0.5$. We therefore derive constraints or sensitivities in this four-dimensional parameter space, focusing in particular on how large a mass splitting can be probed for sub-GeV DM, which is typically only weakly constrained by direct-detection experiments.

Fig. 3 presents the sensitivity in the m_{χ_1} - δ_{DM} plane for two representative choices of the mediator-to-DM mass

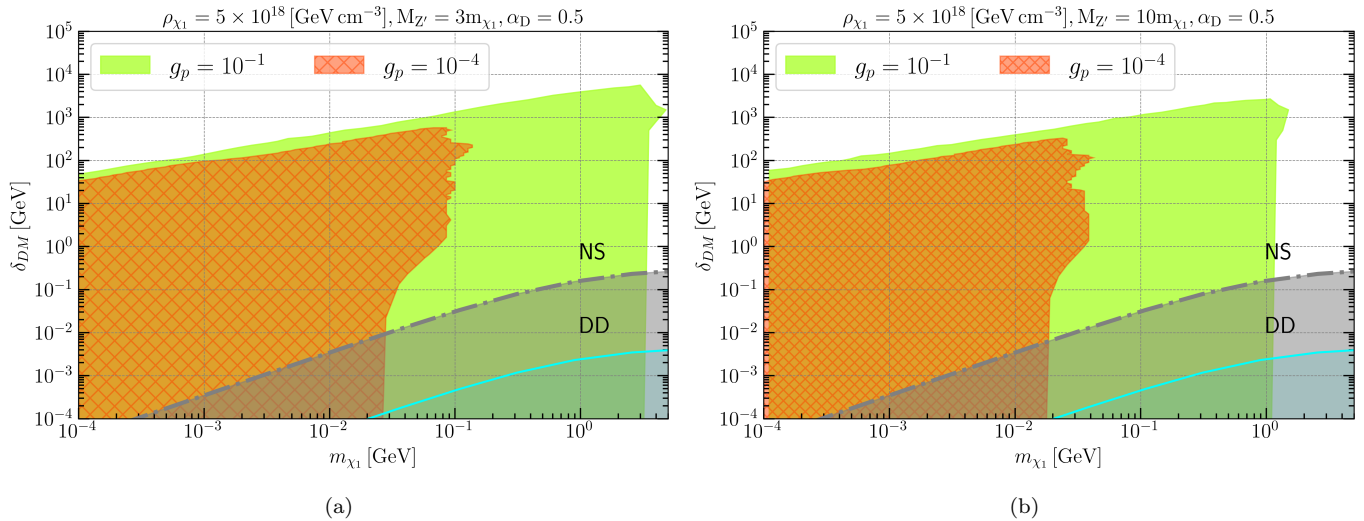


FIG. 3: Sensitivity on mass splitting δ_{DM} as a function of DM mass m_{χ_1} for two benchmark of proton-DM coupling $g_p = 0.1$ (green region) and 10^{-4} (orange region). Left and right panel stand for the mediator to DM mass ratios $M_{Z'}/m_{\chi_1} = 3$ and $M_{Z'}/m_{\chi_1} = 10$, respectively. For comparison, complementary constraints from neutron star (NS) and direct detection (DD) experiments are also shown as gray and cyan shaded regions, respectively.

ratio, $M_{Z'}/m_{\chi_1} = 3$ (left panel) and $M_{Z'}/m_{\chi_1} = 10$ (right panel), and two benchmark couplings $g_p = 10^{-1}$ (green) and $g_p = 10^{-4}$ (orange). For fixed DM mass, the sensitivity remains strong only up to a certain value of δ_{DM} , beyond which it progressively weakens. This behavior has two origins. First, as δ_{DM} increases, Q^2 decreases, which reduces the suppression of the differential cross section as seen in Eqs. 6 and 11. Second, cooling is kinematically allowed only when $s > (m_p + m_{\chi_1} + \delta_{DM})^2$. Consequently, the bounds become weaker for $m_{\chi_1} \lesssim \frac{\delta_{DM}^2 + 2m_p \delta_{DM}}{2T_{p,\min} - 2\delta_{DM}}$ and disappear entirely when $m_{\chi_1} \lesssim \frac{\delta_{DM}^2 + 2m_p \delta_{DM}}{2T_{p,\max} - 2\delta_{DM}}$, where $T_{p,\min}$ and $T_{p,\max}$ denote the minimum and maximum kinetic energies of the proton considered in the cooling analysis. As expected, larger DM-proton coupling allows a large region of the $m_{\chi_1} - \delta_{DM}$ plane to be probed, since the corresponding cross-section is larger and the cooling time scale shorter. Although the DIS contribution can be significant for a heavier mediator mass, a comparison of the two panels shows that a heavier mediator allows sensitivity to smaller DM masses.

The iDM has been investigated in various astrophysical environments, such as neutron stars (NS), as well as in direct detection (DD) experiments. Near a NS, gravitational acceleration can boost χ_1 to $v_{\text{rel}} \approx 0.8c$, enabling efficient energy deposition through scattering [100–103]. Consequently, Cold NSs with surface temperatures of order 2000 K may reveal kinetic heating induced by the deposition of kinetic energy from χ_1 in scattering events, potentially making this scenario accessible to future infrared telescopes⁴. In contrast, the boosted DM scenario offers promising detection prospects in Earth-based experiments, where χ_1 with velocities $v_{\text{rel}} \approx \mathcal{O}(0.1c)$ can induce recoil energies above detector thresholds [20, 51, 104]. Based on the kinematic requirement for DM up-scattering, we define the upper limit on δ_{DM} by imposing the following condition:

$$\delta_{DM} \leq \left(\frac{2m_{\chi_1} m_{\text{SM}}}{\sqrt{1 - v_{\text{rel}}^2}} + m_{\chi_1}^2 + m_{\text{SM}}^2 \right)^{1/2} - m_{\chi_1} - m_{\text{SM}}, \quad (14)$$

where m_{SM} is the mass of the Standard Model (SM) target and v_{rel} is the relative velocity measured in the rest frame of SM target. Correspondingly, in Fig. 3, we show the DM sensitivity reach for NS (gray shaded region) and DD

⁴ For the NS analysis, we assume that χ_1 is in the optically thick regime, such that the capture efficiency is saturated. A detailed study of the resulting observational signatures and detection prospects is beyond the scope of the present work and is left for future investigation.

experiments (cyan shaded region). We see that in the regime of large mass splittings, above a few GeV, conventional direct-detection experiments and astrophysical probes such as neutron stars offer little prospect for discovering iDM. Hence, we conclude that CR cooling in AGN provides sensitivity to inelastic dark matter mass splittings that are orders of magnitude larger than those accessible in conventional searches, reaching well above the TeV scale for DM mass $m_{\chi_1} \sim \mathcal{O}(0.1)$ GeV.

IV. CONCLUSION

In this work, we investigated the sensitivity of CR cooling in the AGN NGC 1068 to sub-GeV inelastic dark matter within a minimal vector-portal framework. The dense DM spike surrounding the SMBH can induce significant energy losses of high-energy CR protons through DM upscattering. Unlike previous analyses that focused mainly on elastic scattering with dipole form factors, we consistently included both elastic and DIS contributions to the cooling rate, demonstrating that DIS becomes dominant at large momentum transfer and substantially enhances the overall cooling effect.

By requiring that the DM-induced cooling timescale not fall below the SM cooling timescale observed in NGC 1068, we derived meaningful constraints on the iDM parameter space. Our results show that AGN cosmic-ray cooling can probe sub-GeV iDM with relatively large mass splittings, extending well beyond the reach of current direct-detection experiments. The sensitivity depends strongly on the mediator mass, the DM–proton coupling, and the structure of the DM spike. Importantly, even when accounting for possible softening of the spike profile due to dynamical evolution effects, the resulting constraints remain competitive and significantly stronger than existing neutron-star and direct-detection bounds over a broad region of parameter space.

Taken together, our study highlights AGNs as powerful astrophysical laboratories for probing non-annihilating sub-GeV inelastic dark matter. The inclusion of DIS contributions is essential for obtaining reliable constraints in the high-energy regime relevant to AGN cosmic rays, and future multimessenger observations offer a promising avenue for further improving the sensitivity to dark-sector interactions.

ACKNOWLEDGMENTS

The work of S.M. is supported by KIAS Individual Grants (PG086002) at Korea Institute for Advanced Study. The work of AR is supported by Basic Science Research Program through the National Research Foundation of Korea (NRF) funded by the Ministry of Education through the Center for Quantum Spacetime (CQUeST) of Sogang University (RS-2020-NR049598) and by the Ministry of Science and ICT with grant number RS-2025-24523022.

Appendix A: Comparison of elastic scattering with dipole form factor, elastic scattering with general form factors and DIS

In Fig. 4, we illustrate the relative importance of the DIS contribution compared to the elastic contribution computed using either the dipole form factor approximation ($F_1(Q^2) = (1 + Q^2/\Lambda^2)^{-2}$) or the more general form-factor treatment ($F_1(Q^2), F_2(Q^2) \neq 0$). For this analysis, we fix the mediator mass to $M_{Z'} = 10 m_{\chi_1}$, while set the reference DM–proton cross section to $\sigma_{\text{DM-p}}^{\text{NR}} = 5 \times 10^{-35}$ cm². The left and right panels differ only in the choice of dark matter mass and mass splitting. We observe that assuming only elastic scattering with the pure dipole form factor (dotted magenta) leads to significantly larger cooling timescales. Including the full elastic contribution with general form factors (green dashed) reduces the cooling timescale appreciably. Nevertheless, the DIS contribution, shown by the red dot-dashed curve, provides the dominant contribution to the cooling timescale over the relevant energy range.

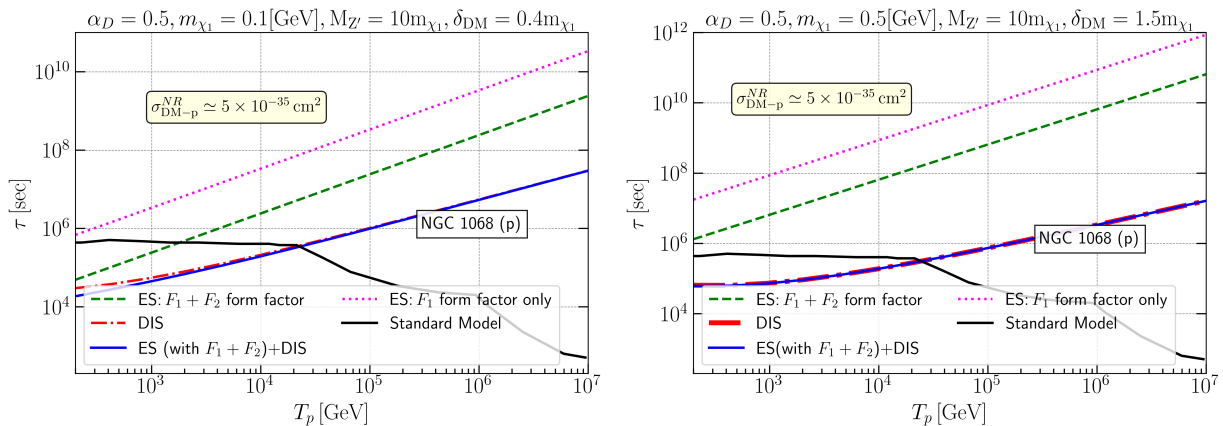


FIG. 4: Comparison of elastic scattering (ES) with dipole form factor, ES with general form factors and deep inelastic scattering (DIS) contribution to cooling time scale for fixed DM mass and fixed DM mass to mediator ratio.

This highlights the importance of the general form factor, compared to the dipole form factor, in elastic scattering, as well as the overall significance of DIS scattering in cosmic-ray cooling.

Appendix B: DM spike uncertainties

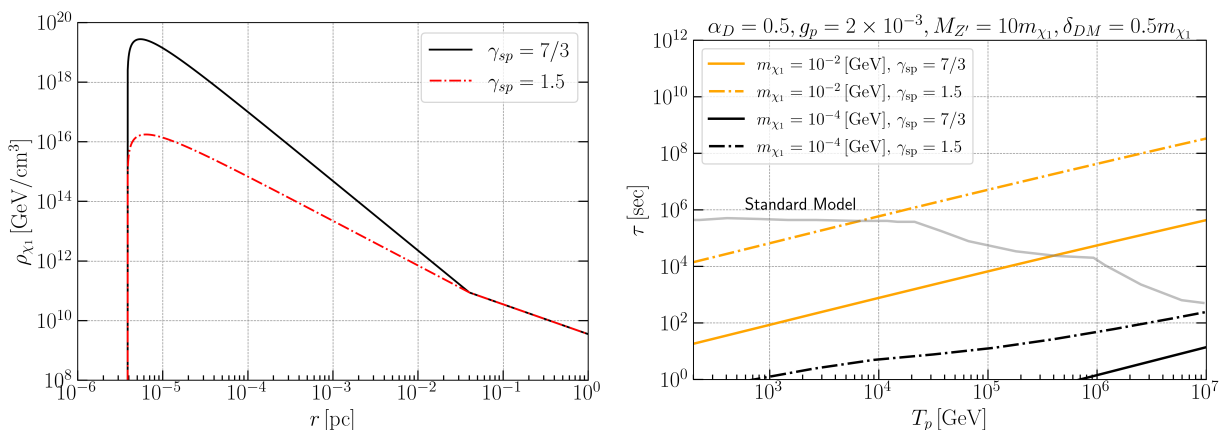


FIG. 5: Left panel: DM distribution in NGC 1068, for different values of spike index γ_{sp} . The black line is the standard case with NFW profile and $\gamma = 1$. Right panel: dependence of spike index on cooling timescales. Orange and black lines stand for DM mass $m_{\chi_1} = 10^{-2}$ GeV and 10^{-4} GeV, respectively, whereas the solid and dot-dashed lines stand for spike index $\gamma_{sp} = 7/3$ and $\gamma_{sp} = 1.5$, respectively.

In addition to self-annihilations, the steepness of the dark matter spike profile can be reduced by several other mechanisms. In particular, galaxy mergers may lead to the formation of supermassive black hole binaries, which transfer energy to the surrounding dark matter spike and consequently soften the density profile. It has also been suggested that gravitational interactions with baryons can heat the dark matter spike, potentially lowering the spike index to values as small as $\gamma_{sp} = 1.5$ [105]. Naturally, such dynamical evolution effects can modify our results. To illustrate their impact, we consider several benchmark choices of γ_{sp} . In the left panel of Fig. 5, we show the dark matter profiles in NGC 1068 for different values of γ_{sp} . Note that the choice $\gamma_{sp} = 7/3$ corresponds to an NFW profile with $\gamma = 1$. Comparing the black and red curves, one observes that the dark matter spike can be substantially

reduced. In the right panel, we show the corresponding impact on the cooling timescale. For this analysis, we consider two dark matter masses, $m_{\chi_1} = 10^{-2}$ GeV (orange curves) and 10^{-4} GeV (black curves), together with spike indices $\gamma_{\text{sp}} = 7/3$ (solid lines) and $\gamma_{\text{sp}} = 1.5$ (dot-dashed lines). We fix the mediator mass and mass splitting to $M_{Z'} = 10, m_{\chi_1}$ and $\delta_{\text{DM}} = 0.5, m_{\chi_1}$. In both benchmark scenarios, there is a clear difference between the cases with $\gamma_{\text{sp}} = 7/3$ and $\gamma_{\text{sp}} = 1.5$. This indicates that the sensitivity obtained in Fig. 3 becomes weaker for $\gamma_{\text{sp}} = 1.5$. More specifically, we find that the sensitivity to the mass splitting is reduced by roughly one to two orders of magnitude, although it still remains stronger than the existing direct-detection and neutron-star constraints.

-
- [1] G. Bertone, D. Hooper, and J. Silk, “Particle dark matter: Evidence, candidates and constraints,” *Phys. Rept.* **405** (2005) 279–390, [arXiv:hep-ph/0404175](#).
 - [2] M. Cirelli, A. Strumia, and J. Zupan, “Dark Matter,” [arXiv:2406.01705 \[hep-ph\]](#).
 - [3] L. Bergström, “Nonbaryonic dark matter: Observational evidence and detection methods,” *Rept. Prog. Phys.* **63** (2000) 793, [arXiv:hep-ph/0002126](#).
 - [4] B. W. Lee and S. Weinberg, “Cosmological Lower Bound on Heavy Neutrino Masses,” *Phys. Rev. Lett.* **39** (1977) 165–168.
 - [5] G. Jungman, M. Kamionkowski, and K. Griest, “Supersymmetric dark matter,” *Phys. Rept.* **267** (1996) 195–373, [arXiv:hep-ph/9506380](#).
 - [6] R. Essig, A. Manalaysay, J. Mardon, P. Sorensen, and T. Volansky, “First Direct Detection Limits on sub-GeV Dark Matter from XENON10,” *Phys. Rev. Lett.* **109** (2012) 021301, [arXiv:1206.2644 \[astro-ph.CO\]](#).
 - [7] **XENON1T** Collaboration, E. Aprile, “The XENON1T Dark Matter Search Experiment,” *Springer Proc. Phys.* **148** (2013) 93–96, [arXiv:1206.6288 \[astro-ph.IM\]](#).
 - [8] **PandaX-II** Collaboration, X. Cui *et al.*, “Dark Matter Results From 54-Ton-Day Exposure of PandaX-II Experiment,” *Phys. Rev. Lett.* **119** no. 18, (2017) 181302, [arXiv:1708.06917 \[astro-ph.CO\]](#).
 - [9] M. J. Dolan, F. Kahlhoefer, and C. McCabe, “Directly detecting sub-GeV dark matter with electrons from nuclear scattering,” *Phys. Rev. Lett.* **121** no. 10, (2018) 101801, [arXiv:1711.09906 \[hep-ph\]](#).
 - [10] N. F. Bell, J. B. Dent, R. F. Lang, J. L. Newstead, and A. C. Ritter, “Observing the Migdal effect from nuclear recoils of neutral particles with liquid xenon and argon detectors,” *Phys. Rev. D* **105** no. 9, (2022) 096015, [arXiv:2112.08514 \[hep-ph\]](#).
 - [11] G. Elor, R. McGehee, and A. Pierce, “Maximizing Direct Detection with Highly Interactive Particle Relic Dark Matter,” *Phys. Rev. Lett.* **130** no. 3, (2023) 031803, [arXiv:2112.03920 \[hep-ph\]](#).
 - [12] **DAMIC-M** Collaboration, I. Arnquist *et al.*, “First Constraints from DAMIC-M on Sub-GeV Dark-Matter Particles Interacting with Electrons,” *Phys. Rev. Lett.* **130** no. 17, (2023) 171003, [arXiv:2302.02372 \[hep-ex\]](#).
 - [13] **SENSEI** Collaboration, P. Adari *et al.*, “First Direct-Detection Results on Sub-GeV Dark Matter Using the SENSEI Detector at SNOLAB,” *Phys. Rev. Lett.* **134** no. 1, (2025) 011804, [arXiv:2312.13342 \[astro-ph.CO\]](#).
 - [14] A. G. De Marchi, A. Granelli, J. Nava, and F. Sala, “Did IceCube discover dark matter around blazars?,” *Phys. Rev. D* **112** no. 4, (2025) 043042, [arXiv:2412.07861 \[astro-ph.HE\]](#).
 - [15] A. N. Baushev, “Extragalactic dark matter and direct detection experiments,” *Astrophys. J.* **771** (2013) 117, [arXiv:1208.0392 \[astro-ph.CO\]](#).
 - [16] G. Besla, A. Peter, and N. Garavito-Camargo, “The highest-speed local dark matter particles come from the Large Magellanic Cloud,” *JCAP* **11** (2019) 013, [arXiv:1909.04140 \[astro-ph.GA\]](#).
 - [17] G. Herrera and A. Ibarra, “Direct detection of non-galactic light dark matter,” *Phys. Lett. B* **820** (2021) 136551, [arXiv:2104.04445 \[hep-ph\]](#).
 - [18] G. Herrera, A. Ibarra, and S. Shirai, “Enhanced prospects for direct detection of inelastic dark matter from a non-galactic diffuse component,” *JCAP* **04** (2023) 026, [arXiv:2301.00870 \[hep-ph\]](#).
 - [19] A. Smith-Orlik *et al.*, “The impact of the Large Magellanic Cloud on dark matter direct detection signals,” *JCAP* **10** (2023) 070, [arXiv:2302.04281 \[astro-ph.GA\]](#).
 - [20] T. Bringmann and M. Pospelov, “Novel direct detection constraints on light dark matter,” *Phys. Rev. Lett.* **122** no. 17, (2019) 171801, [arXiv:1810.10543 \[hep-ph\]](#).

- [21] Y. Ema, F. Sala, and R. Sato, “Light Dark Matter at Neutrino Experiments,” *Phys. Rev. Lett.* **122** no. 18, (2019) 181802, [arXiv:1811.00520 \[hep-ph\]](#).
- [22] J. Alvey, M. Campos, M. Fairbairn, and T. You, “Detecting Light Dark Matter via Inelastic Cosmic Ray Collisions,” *Phys. Rev. Lett.* **123** (2019) 261802, [arXiv:1905.05776 \[hep-ph\]](#).
- [23] J.-W. Wang, A. Granelli, and P. Ullio, “Direct Detection Constraints on Blazar-Boosted Dark Matter,” *Phys. Rev. Lett.* **128** no. 22, (2022) 221104, [arXiv:2111.13644 \[astro-ph.HE\]](#).
- [24] K. Agashe, Y. Cui, L. Necib, and J. Thaler, “(In)direct Detection of Boosted Dark Matter,” *JCAP* **10** (2014) 062, [arXiv:1405.7370 \[hep-ph\]](#).
- [25] D. Kim, J.-C. Park, and S. Shin, “Dark Matter “Collider” from Inelastic Boosted Dark Matter,” *Phys. Rev. Lett.* **119** no. 16, (2017) 161801, [arXiv:1612.06867 \[hep-ph\]](#).
- [26] A. Das and M. Sen, “Boosted dark matter from diffuse supernova neutrinos,” *Phys. Rev. D* **104** no. 7, (2021) 075029, [arXiv:2104.00027 \[hep-ph\]](#).
- [27] C. V. Cappiello, N. P. A. Kozar, and A. C. Vincent, “Dark matter from Monogem,” *Phys. Rev. D* **107** no. 3, (2023) 035003, [arXiv:2210.09448 \[hep-ph\]](#).
- [28] C. A. Argüelles, V. Muñoz, I. M. Shoemaker, and V. Takhistov, “Hadrophilic light dark matter from the atmosphere,” *Phys. Lett. B* **833** (2022) 137363, [arXiv:2203.12630 \[hep-ph\]](#).
- [29] Y.-H. Lin, W.-H. Wu, M.-R. Wu, and H. T.-K. Wong, “Searching for Afterglow: Light Dark Matter Boosted by Supernova Neutrinos,” *Phys. Rev. Lett.* **130** no. 11, (2023) 111002, [arXiv:2206.06864 \[hep-ph\]](#).
- [30] Y. Hochberg, E. Kuflik, T. Volansky, and J. G. Wacker, “Mechanism for Thermal Relic Dark Matter of Strongly Interacting Massive Particles,” *Phys. Rev. Lett.* **113** (2014) 171301, [arXiv:1402.5143 \[hep-ph\]](#).
- [31] P. J. Fitzpatrick, H. Liu, T. R. Slatyer, and Y.-D. Tsai, “New pathways to the relic abundance of vector-portal dark matter,” *Phys. Rev. D* **106** no. 8, (2022) 083517, [arXiv:2011.01240 \[hep-ph\]](#).
- [32] S.-Y. Ho, P. Ko, and C.-T. Lu, “Scalar and fermion two-component SIMP dark matter with an accidental Z_4 symmetry,” *JHEP* **03** (2022) 005, [arXiv:2201.06856 \[hep-ph\]](#).
- [33] B. Bhattacharjee, S. Matsumoto, S. Mukhopadhyay, and M. M. Nojiri, “Phenomenology of light fermionic asymmetric dark matter,” *JHEP* **10** (2013) 032, [arXiv:1306.5878 \[hep-ph\]](#).
- [34] E. Izaguirre, G. Krnjaic, P. Schuster, and N. Toro, “Analyzing the Discovery Potential for Light Dark Matter,” *Phys. Rev. Lett.* **115** no. 25, (2015) 251301, [arXiv:1505.00011 \[hep-ph\]](#).
- [35] S.-Y. Ho, “An asymmetric SIMP dark matter model,” *JHEP* **10** (2022) 182, [arXiv:2207.13373 \[hep-ph\]](#).
- [36] E. Frangipane, S. Gori, and B. Shakya, “Dark matter freeze-in with a heavy mediator: beyond the EFT approach,” *JHEP* **09** (2022) 083, [arXiv:2110.10711 \[hep-ph\]](#).
- [37] P. N. Bhattiprolu, G. Elor, R. McGehee, and A. Pierce, “Freezing-in hadrophilic dark matter at low reheating temperatures,” *JHEP* **01** (2023) 128, [arXiv:2210.15653 \[hep-ph\]](#).
- [38] D. Tucker-Smith and N. Weiner, “Inelastic dark matter,” *Phys. Rev. D* **64** (2001) 043502, [arXiv:hep-ph/0101138](#).
- [39] D. Tucker-Smith and N. Weiner, “The Status of inelastic dark matter,” *Phys. Rev. D* **72** (2005) 063509, [arXiv:hep-ph/0402065](#).
- [40] S. Chang, G. D. Kribs, D. Tucker-Smith, and N. Weiner, “Inelastic Dark Matter in Light of DAMA/LIBRA,” *Phys. Rev. D* **79** (2009) 043513, [arXiv:0807.2250 \[hep-ph\]](#).
- [41] R. Bernabei *et al.*, “Final model independent result of DAMA/LIBRA-phase1,” *Eur. Phys. J. C* **73** (2013) 2648, [arXiv:1308.5109 \[astro-ph.GA\]](#).
- [42] J. R. Jordan, Y. Kahn, G. Krnjaic, M. Moschella, and J. Spitz, “Signatures of Pseudo-Dirac Dark Matter at High-Intensity Neutrino Experiments,” *Phys. Rev. D* **98** no. 7, (2018) 075020, [arXiv:1806.05185 \[hep-ph\]](#).
- [43] A. Berlin, S. Gori, P. Schuster, and N. Toro, “Dark Sectors at the Fermilab SeaQuest Experiment,” *Phys. Rev. D* **98** no. 3, (2018) 035011, [arXiv:1804.00661 \[hep-ph\]](#).
- [44] B. Batell, J. Berger, L. Darmé, and C. Frugiuele, “Inelastic dark matter at the Fermilab Short Baseline Neutrino Program,” *Phys. Rev. D* **104** no. 7, (2021) 075026, [arXiv:2106.04584 \[hep-ph\]](#).
- [45] M. Mongillo, A. Abdullahi, B. B. Oberhauser, P. Crivelli, M. Hostert, D. Massaro, L. M. Bueno, and S. Pascoli, “Constraining light thermal inelastic dark matter with NA64,” *Eur. Phys. J. C* **83** no. 5, (2023) 391, [arXiv:2302.05414 \[hep-ph\]](#).
- [46] E. Izaguirre, G. Krnjaic, and B. Shuve, “Discovering Inelastic Thermal-Relic Dark Matter at Colliders,” *Phys. Rev. D* **93** no. 6, (2016) 063523, [arXiv:1508.03050 \[hep-ph\]](#).

- [47] T. Schwetz and J. Zupan, “Dark Matter attempts for CoGeNT and DAMA,” *JCAP* **08** (2011) 008, [arXiv:1106.6241 \[hep-ph\]](#).
- [48] J. Bramante, P. J. Fox, G. D. Kribs, and A. Martin, “Inelastic frontier: Discovering dark matter at high recoil energy,” *Phys. Rev. D* **94** no. 11, (2016) 115026, [arXiv:1608.02662 \[hep-ph\]](#).
- [49] M. Baryakhtar, A. Berlin, H. Liu, and N. Weiner, “Electromagnetic signals of inelastic dark matter scattering,” *JHEP* **06** (2022) 047, [arXiv:2006.13918 \[hep-ph\]](#).
- [50] N. Song, S. Nagorny, and A. C. Vincent, “Pushing the frontier of WIMPy inelastic dark matter: Journey to the end of the periodic table,” *Phys. Rev. D* **104** no. 10, (2021) 103032, [arXiv:2104.09517 \[hep-ph\]](#).
- [51] N. F. Bell, J. B. Dent, B. Dutta, S. Ghosh, J. Kumar, J. L. Newstead, and I. M. Shoemaker, “Cosmic-ray upscattered inelastic dark matter,” *Phys. Rev. D* **104** (2021) 076020, [arXiv:2108.00583 \[hep-ph\]](#).
- [52] J. Eby, P. J. Fox, and G. D. Kribs, “Earth-catalyzed detection of magnetic inelastic dark matter with photons in large underground detectors,” *JHEP* **06** (2024) 165, [arXiv:2312.08478 \[hep-ph\]](#).
- [53] S. Chatterjee and R. Laha, “Explorations of pseudo-Dirac dark matter having keV splittings and interacting via transition electric and magnetic dipole moments,” *Phys. Rev. D* **107** no. 8, (2023) 083036, [arXiv:2202.13339 \[hep-ph\]](#).
- [54] S. Kang, S. Scopel, and G. Tomar, “Low-mass constraints on WIMP effective models of inelastic scattering using the Migdal effect,” *JCAP* **01** (2025) 035, [arXiv:2407.16187 \[hep-ph\]](#).
- [55] T. Emken, J. Frerick, S. Heeba, and F. Kahlhoefer, “Electron recoils from terrestrial upscattering of inelastic dark matter,” *Phys. Rev. D* **105** no. 5, (2022) 055023, [arXiv:2112.06930 \[hep-ph\]](#).
- [56] G. D. V. Garcia, F. Kahlhoefer, M. Ovchinnikov, and T. Schwetz, “Not-so-inelastic Dark Matter,” *JHEP* **02** (2025) 127, [arXiv:2405.08081 \[hep-ph\]](#).
- [57] R. Essig *et al.*, “Snowmass2021 Cosmic Frontier: The landscape of low-threshold dark matter direct detection in the next decade,” in *Snowmass 2021*. 3, 2022. [arXiv:2203.08297 \[hep-ph\]](#).
- [58] Z. Yun, J. Sun, B. Zhu, and X. Liu, “Probing inelastic signatures of dark matter detection via polarized nucleus*,” *Chin. Phys. C* **48** no. 10, (2024) 103106, [arXiv:2309.01203 \[hep-ph\]](#).
- [59] J. Li, L. Su, L. Wu, and B. Zhu, “Spin-dependent sub-GeV inelastic dark matter-electron scattering and Migdal effect. Part I. Velocity independent operator,” *JCAP* **04** (2023) 020, [arXiv:2210.15474 \[hep-ph\]](#).
- [60] N. F. Bell, J. B. Dent, B. Dutta, J. Kumar, and J. L. Newstead, “Indirect detection of low mass dark matter in direct detection experiments with inelastic scattering,” *Phys. Rev. D* **106** no. 10, (2022) 103016, [arXiv:2208.08020 \[hep-ph\]](#).
- [61] Y. Gu, L. Wu, and B. Zhu, “Detection of inelastic dark matter via electron recoils in SENSEI,” *Phys. Rev. D* **106** no. 7, (2022) 075004, [arXiv:2203.06664 \[hep-ph\]](#).
- [62] F. M. Rieger, “Active Galactic Nuclei as Potential Sources of Ultra-High Energy Cosmic Rays,” *Universe* **8** no. 11, (2022) 607, [arXiv:2211.12202 \[astro-ph.HE\]](#).
- [63] K. Murase and F. W. Stecker, “Chapter 10: High-Energy Neutrinos from Active Galactic Nuclei,” [arXiv:2202.03381 \[astro-ph.HE\]](#).
- [64] **IceCube** Collaboration, R. Abbasi *et al.*, “Evidence for neutrino emission from the nearby active galaxy NGC 1068,” *Science* **378** no. 6619, (2022) 538–543, [arXiv:2211.09972 \[astro-ph.HE\]](#).
- [65] M. Ajello, K. Murase, and A. McDaniel, “Disentangling the Hadronic Components in NGC 1068,” *Astrophys. J. Lett.* **954** no. 2, (2023) L49, [arXiv:2307.02333 \[astro-ph.HE\]](#).
- [66] **IceCube**, **Fermi-LAT**, **MAGIC**, **AGILE**, **ASAS-SN**, **HAWC**, **H.E.S.S.**, **INTEGRAL**, **Kanata**, **Kiso**, **Kapteyn**, **Liverpool Telescope**, **Subaru**, **Swift NuSTAR**, **VERITAS**, **VLA/17B-403** Collaboration, M. G. Aartsen *et al.*, “Multimessenger observations of a flaring blazar coincident with high-energy neutrino IceCube-170922A,” *Science* **361** no. 6398, (2018) eaat1378, [arXiv:1807.08816 \[astro-ph.HE\]](#).
- [67] **IceCube** Collaboration, M. G. Aartsen *et al.*, “Neutrino emission from the direction of the blazar TXS 0506+056 prior to the IceCube-170922A alert,” *Science* **361** no. 6398, (2018) 147–151, [arXiv:1807.08794 \[astro-ph.HE\]](#).
- [68] **MAGIC** Collaboration, S. Ansoldi *et al.*, “The blazar TXS 0506+056 associated with a high-energy neutrino: insights into extragalactic jets and cosmic ray acceleration,” *Astrophys. J. Lett.* **863** (2018) L10, [arXiv:1807.04300 \[astro-ph.HE\]](#).
- [69] A. Keivani *et al.*, “A Multimessenger Picture of the Flaring Blazar TXS 0506+056: implications for High-Energy Neutrino Emission and Cosmic Ray Acceleration,” *Astrophys. J.* **864** no. 1, (2018) 84, [arXiv:1807.04537 \[astro-ph.HE\]](#).
- [70] P. Padovani, F. Oikonomou, M. Petropoulou, P. Giommi, and E. Resconi, “TXS 0506+056, the first cosmic neutrino

- source, is not a BL Lac,” *Mon. Not. Roy. Astron. Soc.* **484** no. 1, (2019) L104–L108, [arXiv:1901.06998 \[astro-ph.HE\]](#).
- [71] P. Gondolo and J. Silk, “Dark matter annihilation at the galactic center,” *Phys. Rev. Lett.* **83** (1999) 1719–1722, [arXiv:astro-ph/9906391](#).
- [72] P. Ullio, H. Zhao, and M. Kamionkowski, “A Dark matter spike at the galactic center?,” *Phys. Rev. D* **64** (2001) 043504, [arXiv:astro-ph/0101481](#).
- [73] T. Lacroix, M. Karami, A. E. Broderick, J. Silk, and C. Boehm, “Unique probe of dark matter in the core of M87 with the Event Horizon Telescope,” *Phys. Rev. D* **96** no. 6, (2017) 063008, [arXiv:1611.01961 \[astro-ph.GA\]](#).
- [74] G. Herrera and K. Murase, “Probing light dark matter through cosmic-ray cooling in active galactic nuclei,” *Phys. Rev. D* **110** no. 1, (2024) L011701, [arXiv:2307.09460 \[hep-ph\]](#).
- [75] R. A. Gustafson, G. Herrera, M. Mukhopadhyay, K. Murase, and I. M. Shoemaker, “Cosmic-ray boosted inelastic dark matter from neutrino-emitting active galactic nuclei,” [arXiv:2508.20984 \[hep-ph\]](#).
- [76] L. Li, C.-T. Lu, A. K. Mishra, L. Su, and L. Wu, “Enhanced Cosmic-Ray Cooling in AGN from Dark Matter Deep Inelastic Scattering,” [arXiv:2509.11906 \[hep-ph\]](#).
- [77] R. A. Gustafson, G. Herrera, M. Mukhopadhyay, K. Murase, and I. M. Shoemaker, “Cosmic-ray cooling in active galactic nuclei as a new probe of inelastic dark matter,” *Phys. Rev. D* **111** no. 12, (2025) L121303, [arXiv:2408.08947 \[hep-ph\]](#).
- [78] A. K. Mishra, N. Liu, and C.-T. Lu, “Probing gauged U(1) sub-GeV dark matter via cosmic ray cooling in active galactic nuclei,” *Phys. Dark Univ.* **49** (2025) 102050, [arXiv:2504.03409 \[hep-ph\]](#).
- [79] G. Bélanger, M. Mitra, R. Padhan, and A. Roy, “Illuminating scalar dark matter co-scattering in EFT with monophoton signatures,” *JHEP* **01** (2026) 007, [arXiv:2508.06040 \[hep-ph\]](#).
- [80] K. Griest and D. Seckel, “Three exceptions in the calculation of relic abundances,” *Phys. Rev. D* **43** (1991) 3191–3203.
- [81] M. Garny, J. Heisig, B. Lülff, and S. Vogl, “Coannihilation without chemical equilibrium,” *Phys. Rev. D* **96** no. 10, (2017) 103521, [arXiv:1705.09292 \[hep-ph\]](#).
- [82] G. B. Gelmini and P. Gondolo, “Neutralino with the right cold dark matter abundance in (almost) any supersymmetric model,” *Phys. Rev. D* **74** (2006) 023510, [arXiv:hep-ph/0602230](#).
- [83] N. Bernal, K. Deka, and M. Losada, “Thermal dark matter with low-temperature reheating,” *JCAP* **09** (2024) 024, [arXiv:2406.17039 \[hep-ph\]](#).
- [84] A. Roy and R. Sahu, “Scrutinizing fermionic Dark Matter in scotogenic model with low reheating temperature,” *JCAP* **03** (2026) 014, [arXiv:2508.14726 \[hep-ph\]](#).
- [85] G. Bélanger, N. Bernal, and A. Pukhov, “Z'-mediated dark matter with low-temperature reheating,” *JHEP* **03** (2025) 079, [arXiv:2412.12303 \[hep-ph\]](#).
- [86] P. G. Ferreira and M. Joyce, “Cosmology with a primordial scaling field,” *Phys. Rev. D* **58** (1998) 023503, [arXiv:astro-ph/9711102](#).
- [87] M. Joyce, “Electroweak Baryogenesis and the Expansion Rate of the Universe,” *Phys. Rev. D* **55** (1997) 1875–1878, [arXiv:hep-ph/9606223](#).
- [88] F. D’Eramo, N. Fernandez, and S. Profumo, “When the Universe Expands Too Fast: Relentless Dark Matter,” *JCAP* **05** (2017) 012, [arXiv:1703.04793 \[hep-ph\]](#).
- [89] K. Murase, S. S. Kimura, and P. Meszaros, “Hidden Cores of Active Galactic Nuclei as the Origin of Medium-Energy Neutrinos: Critical Tests with the MeV Gamma-Ray Connection,” *Phys. Rev. Lett.* **125** no. 1, (2020) 011101, [arXiv:1904.04226 \[astro-ph.HE\]](#).
- [90] D. F. G. Fiorillo, L. Comisso, E. Peretti, M. Petropoulou, and L. Sironi, “A Magnetized Strongly Turbulent Corona as the Source of Neutrinos from NGC 1068,” *Astrophys. J.* **974** no. 1, (2024) 75, [arXiv:2407.01678 \[astro-ph.HE\]](#).
- [91] D. F. G. Fiorillo, L. Comisso, E. Peretti, M. Petropoulou, and L. Sironi, “The Contribution of Turbulent Active Galactic Nucleus Coronae to the Diffuse Neutrino Flux,” *Astrophys. J.* **989** no. 2, (2025) 215, [arXiv:2504.06336 \[astro-ph.HE\]](#).
- [92] K. Murase, “Hidden Hearts of Neutrino Active Galaxies,” *Astrophys. J. Lett.* **941** no. 1, (2022) L17, [arXiv:2211.04460 \[astro-ph.HE\]](#).
- [93] J. F. Navarro, C. S. Frenk, and S. D. M. White, “A Universal density profile from hierarchical clustering,” *Astrophys. J.* **490** (1997) 493–508, [arXiv:astro-ph/9611107](#).
- [94] J. F. Navarro, C. S. Frenk, and S. D. M. White, “The Structure of cold dark matter halos,” *Astrophys. J.* **462** (1996) 563–575, [arXiv:astro-ph/9508025](#).
- [95] A. Ambrosone, M. Chianese, D. F. G. Fiorillo, A. Marinelli, and G. Miele, “Starburst Galactic Nuclei as Light Dark

- Matter Laboratories,” *Phys. Rev. Lett.* **131** no. 11, (2023) 111003, [arXiv:2210.05685 \[astro-ph.HE\]](#).
- [96] C. F. Perdrisat, V. Punjabi, and M. Vanderhaeghen, “Nucleon Electromagnetic Form Factors,” *Prog. Part. Nucl. Phys.* **59** (2007) 694–764, [arXiv:hep-ph/0612014](#).
- [97] R. G. Sachs, “High-Energy Behavior of Nucleon Electromagnetic Form Factors,” *Phys. Rev.* **126** (1962) 2256–2260.
- [98] J. J. Kelly, “Simple parametrization of nucleon form factors,” *Phys. Rev. C* **70** (2004) 068202.
- [99] A. Buckley, J. Ferrando, S. Lloyd, K. Nordström, B. Page, M. Rufenacht, M. Schönherr, and G. Watt, “LHAPDF6: parton density access in the LHC precision era,” *Eur. Phys. J. C* **75** (2015) 132, [arXiv:1412.7420 \[hep-ph\]](#).
- [100] N. F. Bell, G. Busoni, S. Robles, and M. Virgato, “Improved Treatment of Dark Matter Capture in Neutron Stars,” *JCAP* **09** (2020) 028, [arXiv:2004.14888 \[hep-ph\]](#).
- [101] N. F. Bell, G. Busoni, and S. Robles, “Heating up Neutron Stars with Inelastic Dark Matter,” *JCAP* **09** (2018) 018, [arXiv:1807.02840 \[hep-ph\]](#).
- [102] G. Alvarez, A. Joglekar, M. Phoroutan-Mehr, and H.-B. Yu, “Heating neutron stars with inelastic dark matter and relativistic targets,” *Phys. Rev. D* **107** no. 10, (2023) 103024, [arXiv:2301.08767 \[hep-ph\]](#).
- [103] A. Roy, P. Sanyal, and S. Scopel, “Dark Photon mediated Inelastic Dark Matter in Cosmology, Astrophysics and Colliders,” [arXiv:2602.18051 \[hep-ph\]](#).
- [104] G. F. Giudice, D. Kim, J.-C. Park, and S. Shin, “Inelastic Boosted Dark Matter at Direct Detection Experiments,” *Phys. Lett. B* **780** (2018) 543–552, [arXiv:1712.07126 \[hep-ph\]](#).
- [105] D. Merritt, S. Harfst, and G. Bertone, “Collisionally Regenerated Dark Matter Structures in Galactic Nuclei,” *Phys. Rev. D* **75** (2007) 043517, [arXiv:astro-ph/0610425](#).